OPEN ACCESS

Materials Chemistry ARTICLE

The Innovation Materials

Weak emissive D-O-A organic phosphor: Exceptional matrix-free sensitization in MR-TADF OLEDs

Lulin Xu,[1,5] Shuai Xiao,[1,2,5] Ying Yang,[1,2] Han Si,[1,*] Changsheng Shi,[3] Huaiyi Ding,[3] Ning Sun,[3] Liming Ding,[4,*] and Junqiao Ding[1,2,*]

*Correspondence: sihan94720@outlook.com (H.S.); ding@gdut.edu.cn (L.D.); dingjunqiao@ynu.edu.cn (J.D.)

Received: November 12, 2025; Accepted: March 4, 2026; Published Online: March 4, 2026; https://doi.org/10.59717/j.xinn-mater.2026.100210

GRAPHICAL ABSTRACT

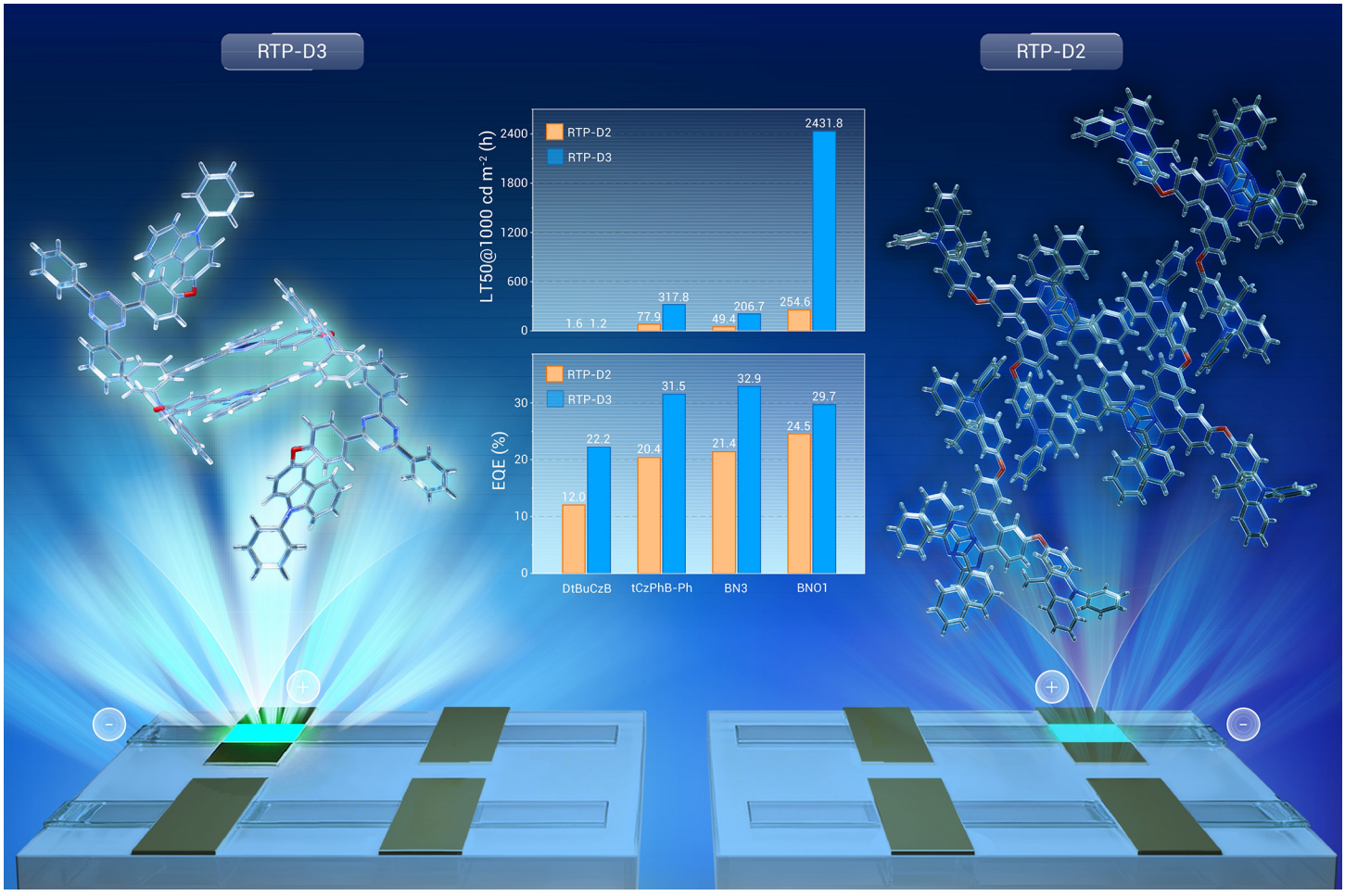

PUBLIC SUMMARY

- A weakly emissive D–O–A organic phosphor is developed to act as an efficient sensitizer for MR–TADF emitters.
- High-performance narrowband electroluminescence is achieved ranging from sky blue to red.
- The exceptional results break a habitual thinking that the best sensitizer should be the best emitter.

ARTICLE Materials Chemistry

www.the-innovation.org/the-innovation-materials

Weak emissive D-O-A organic phosphor: Exceptional matrix-free sensitization in MR-TADF OLEDs

Lulin Xu,[1,5] Shuai Xiao,[1,2,5] Ying Yang,[1,2] Han Si,[1,*] Changsheng Shi,[3] Huaiyi Ding,[3] Ning Sun,[3] Liming Ding,[4,*] and Junqiao Ding[1,2,*]

[1]Key Laboratory of Medicinal Chemistry for Natural Resource, Ministry of Education; School of Chemical Science and Technology, Yunnan University; National Center for International Joint Research of Photoelectronic Energy Materials and Application, Kunming 650091, China

[2]Southwest United Graduate School, Kunming 650092, China

[3]School of Physics and Astronomy, Yunnan University, Kunming 650091, China

[4]School of Chemical Engineering and Light Industry, Guangdong University of Technology, Guangzhou 510006, China

[5]These authors contributed equally

*Correspondence: sihan94720@outlook.com (H.S.); ding@gdut.edu.cn (L.D.); dingjunqiao@ynu.edu.cn (J.D.)

Received: November 12, 2025; Accepted: March 4, 2026; Published Online: March 4, 2026; https://doi.org/10.59717/j.xinn-mater.2026.100210

Citation: Xu L., Xiao S., Yang Y., et al. (2026). Weak emissive D-O-A organic phosphor: Exceptional matrix-free sensitization in MR-TADF OLEDs. *The Innovation Materials* **4**:100210.

D-O-A organic phosphors showing strong aggregation-induced room-temperature phosphorescence (RTP) have been successfully demonstrated as the ideal matrix-free sensitizers for MR-TADF OLEDs. However, weak emissive ones still remain unexplored according to a habitual thinking that the best sensitizer should be the best emitter. Herein, a poor RTP emitter named RTP-D3 is newly developed based on carbazole as the donor, triazine as the acceptor and oxygen as the bridge. In spite of the extremely low photoluminescence quantum yield, RTP-D3 can sensitize the terminal MR-TADF molecules effectively and universally because of favored π-π and C-H···π intermolecular interactions among triazine moieties and thus a balanced charge transport. Consequently, high performance sky-blue, green, yellow and red narrowband electroluminescence is realized together with a state-of-art external quantum efficiency of 22.2% (49.2 cd/A, 55.2 lm/W), 31.5% (105.1 cd/A, 113.9 lm/W), 32.9% (112.4 cd/A, 133.3 lm/W) and 29.7% (55.4 cd/A, 66.9 lm/W) as well as Commission Internationale de l'Eclairage (CIE) coordinates of (0.12, 0.48), (0.26, 0.70), (0.45, 0.54) and (0.61, 0.39), respectively. The exceptional results break a conventional blind spot about RTP sensitizer, highlighting that the less emissive D-O-A organic phosphors are also suitable for the best matrix-free sensitization in MR-TADF OLEDs.

INTRODUCTION

Since the first report in 2016,[1] multiresonance thermally activated delayed fluorescence (MR-TADF) emitters have attracted a growing interest towards the ultrahigh definition displays.[2] Due to the complementary resonance effects, they exhibit not only a narrowband emission with small full width at half maximum (FWHM < 40 nm), but also a large oscillator strength with nearly unity photoluminescence (PL) quantum yield (Φ_{PL}).[3-7] Nowadays a number of efficient MR-TADF emitters have been developed to show tunable emissive colors in the whole visible region.[8-16] Given their moderate reverse intersystem crossing (RISC) rates (about 10^5 s^{-1}), unfortunately, they suffer from insufficient harvesting of triplet excitons under electrical excitation, and thus poor device performance of organic light-emitting diodes (OLEDs).[17] To solve such a problem, TADF molecules are generally incorporated as the sensitizers for MR-TADF OLEDs.[18-20] In this case, a high-triplet-energy matrix is often implemented alongside the TADF sensitizers because of their severe concentration quenching.[21-23] Albeit the success, the requirement for a high-triplet-energy matrix may inevitably bring about unwanted energy loss from matrix to sensitizer during energy transfer. Accordingly, the driving voltage is increased, leading to reduced power efficiency and device stability. Second, the search for an appropriate matrix is not an easy task, especially for blue MR-TADF emitters. Therefore, matrix-free sensitization is highly desirable from a device perspective, where the high-triplet-energy matrix is not needed any longer.[24,25]

With this idea in mind, matrix-free MR-TADF OLEDs have been introduced by adopting TADF sensitizers in the absence of significant concentration quenching.[26,27] However, the expansion is further hindered owing to the scarcity of the best TADF emitters with such a specific concentration dependence.[28-30] As an alternative, organic room-temperature phosphorescence (RTP) molecules do have a great potential in matrix-free MR-TADF OLEDs (Figure 1A).[31,32] First, they tend to give a much brighter RTP in neat film than in doped film because of the suppressed non-radiative decay. Second, most of triplet excitons (75% under electric excitation) can be transferred to MR-TADF emitter via a direct Förster resonance energy transfer (FRET). It is quite different from TADF sensitization, in which triplet excitons must be up-converted to singlet ones through a slow RISC (k_{RISC} = 10^5-10^6 s^{-1}) followed by FRET. Third, the generated 25% singlet excitons is either transferred directly or spin flip to triplet excitons via a fast ISC (k_{ISC} = 10^7-10^8 s^{-1}), whose energy is then harvested by MR-TADF emitter. From these point of views, RTP molecules are capable of aggregation-induced electroluminescence (AIEL) and favored exciton utilization in matrix-free sensitization compared with TADF counterparts. For example, we have recently reported a D-O-A organic phosphor RTP-D2 (2-(4-(4,6-diphenyl-1,3,5-triazin-2-yl)phenoxy)-9,9-dimethyl-10-phenyl-9,10-dihydroacridine) based on acridine as the electron donor (D), triazine as the electron acceptor (A) and oxygen (O) as the bridge between them. It is found to give an exciting aggregation-induced RTP especially in EL.[33] As a consequence, RTP-D2 itself could sensitize the terminal MR-TADF emitter without any additional high-triplet-energy matrix, and realize a bright narrowband EL with a maximum external quantum efficiency (EQE) of 26.4% and a small FWHM of 26 nm.

According to a habitual thinking, the best sensitizer should be the best emitter.[34] Reasonably, RTP-D2 is strong emissive with a high film Φ_{PL} of 77.5%, and acts as an ideal matrix-free sensitizer in MR-TADF OLEDs. On the contrary, what about weak emissive D-O-A organic phosphors that still remain unexplored? To unveil this doubt, herein we delicately design a novel RTP molecule RTP-D3 (3-(4-(4,6-diphenyl-1,3,5-triazin-2-yl)phenoxy)-9-phenyl-9H-carbazole) by replacing acridine with carbazole (Figure 1B). Such a tiny modification endows RTP-D3 with a poor aggregation-induced RTP (Φ_{PL} = 12.8%). Nonetheless, RTP-D3 is able to be utilized as the perfect and universal matrix-free sensitizer for multichromic MR-TADF emitters. In particular, high performance sky-blue, green, yellow and red narrowband EL are achieved successfully, revealing a state-of-art EQE of 22.2% (49.2 cd/A, 55.2 lm/W), 31.5% (105.1 cd/A, 113.9 lm/W), 32.9% (112.4 cd/A, 133.3 lm/W) and 29.7% (55.4 cd/A, 66.9 lm/W) as well as Commission Internationale de l' Eclairage (CIE) coordinates of (0.12, 0.48), (0.26, 0.70), (0.45, 0.54) and (0.61, 0.39), respectively. Compared with the strong emissive RTP-D2, both device efficiency and stability are obviously improved based on the weak emissive RTP-D3, which could be attributed to its favored intermolecular interactions among triazine moieties (π-π stacking and C-H···π interaction) and thus a more balanced charge transport. The exceptional results open a new avenue for RTP sensitizer design, and extend its scope from the best D-O-A organic phosphors to the poor ones.

MATERIALS AND METHODS

Material synthesis and Characterization

RTP-D3 was synthesized in a yield of 88% according to a nucleophilic aromatic substitution reaction between the fluorinated acceptor [2-(4-fluorophenyl)-4,6-diphenyl-1,3,5-triazine] and the hydroxylated donor (9-phenyl-9H-carbazol-3-ol) (Scheme S1).

The chemical structure of RTP-D3 was fully confirmed by ^{1}H NMR, ^{13}C NMR, HR-ESI-MS, elemental analysis and single crystal diffraction (Figures S1-S2 & Table S1). Meanwhile, RTP-D3 possesses an excellent thermal stability with a high decomposition temperature of 382°C (corresponding to a 5% weight loss) and a glass transition temperature of 91°C (Figure S3). And a reversible reduction and quasi-reversible oxidation wave are observed for RTP-D3 during the cathodic and anodic sweeping (Figure S4). With ferrocene/ferrocenium (Fc/Fc^+) as the standard (−4.80 eV under vacuum), the

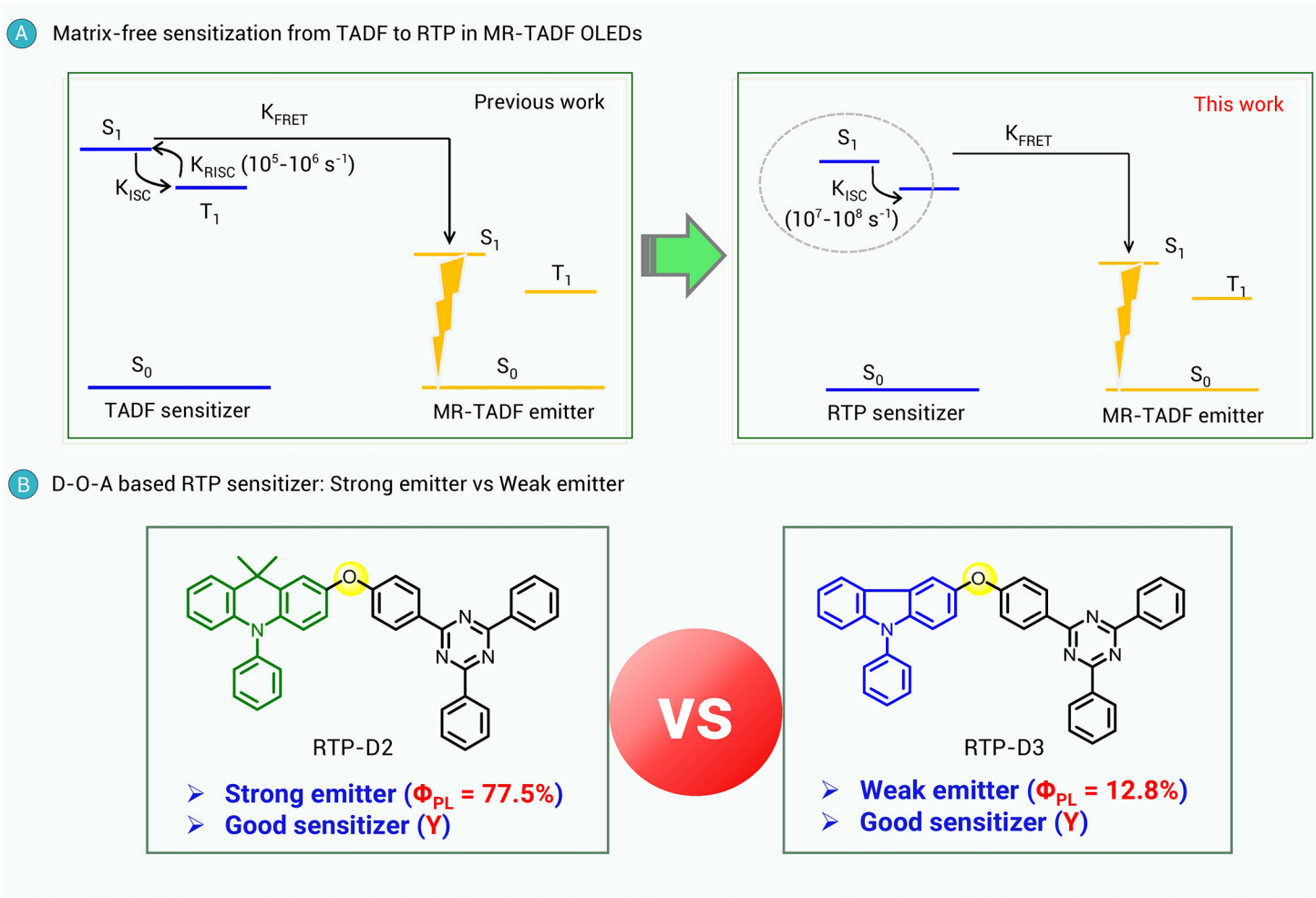

Figure 1. D-O-A based organic phosphors for RTP matrix-free sensitization in MR-TADF OLEDs: strong emitter vs weak emitter.

HOMO and LUMO levels of RTP-D3 are determined to be -5.42 eV and -2.69 eV, respectively. In well agreement with the theoretical calculation, the LUMO is localized on triazine, whereas the HOMO is mainly distributed on carbazole in RTP-D3 and acridine in RTP-D2 (Figure S5). Given the same triazine acceptor and the weaker electron-donating capability of carbazole relative to acridine, reasonably, RTP-D3 shows a close LUMO and a deeper HOMO compared with RTP-D2. Despite this, the observed good electroactivity is believed to favor charge transporting when RTP-D3 is used as the matrix-free sensitizer in MR-TADF OLEDs.

RESULTS

Photophysical property

Figure 2A plots the UV-Vis absorption in dichloromethane, the film PL and RTP spectra for RTP-D3. As can be clearly seen, RTP-D3 exhibits an intense absorption band below 350 nm, corresponding to the n-π* and π-π* transitions of the carbazole and triazine moieties. A weak absorption tail is also discernible above 350 nm, which could be tentatively ascribed to the charge transfer (CT) from carbazole to triazine.[33] In addition, the PL of RTP-D3 is well explored in neat film, since it behaves an aggregation-induced emission (AIE, Figure S6). Due to the replacement of acridine by carbazole, the emission maximum is significantly blue-shifted from 497 nm of RTP-D2 to 437 nm of RTP-D3 (Table 1). And the profile seems to be broad with a FWHM of 82 nm, suggesting that RTP may be involved in the PL of RTP-D3.

To prove this point, the phosphorescent spectrum of RTP-D3 was measured at room temperature with a delay time of 0.1 ms. As expected, an obvious RTP can be detected for RTP-D3, showing an emission maximum of 509 nm as well as a phosphorescent lifetime of 278.5 ns (Figure S7). The RTP nature can be further verified by time-resolved emission spectra (TRES) and temperature-dependent transient PL spectra. When the delay time grows, the TRES is monotonically red-shifted, and finally matches well with the phosphorescent one (Figure 2B). In accordance to the TRES, RTP-D3 has a distinct delayed component in the transient PL recorded at 509 nm, whose intensity is found to be decreased with the increasing temperature (Figure 2C). Together with the negative temperature dependence on the steady-state PL and RTP spectra (Figure S8), these observations imply the existence of RTP for RTP-D3.

Furthermore, TADF is reasonably ruled out according to the transient PL by deliberately varying the detection wavelength (Figure S9). For example, if a detection wavelength of 390 nm is selected to remove the RTP contribution, only prompt fluorescence is observed in the absence of TADF-related delayed component. Hence, we can deduce that the PL of RTP-D3 is composed of fluorescence and RTP. After a Bigaussian fitting, their populations are determined to be 89.4% and 10.6%, respectively (Figure 2E). On one hand, the characteristic D-O-A geometry plays an important role on the RTP generation. In the case of RTP-D3, both the hybridization of n/π orbitals and the large dihedral angle of 66.82° between D and A (Figure S10) would provide enough orbital angular momentum change to compensate the spin angular momentum.[35,36] As a consequence, the intersystem crossing (ISC) from S_1 to T_n becomes spin-allowed, followed by a rapid T_n-to-T_1 internal conversion (IC) and subsequent T_1-to-S_0 radiative decay (Figure 2F). The proposed mechanism is consistent with the moderate but acceptable spin-orbital coupling matrix element (SOCME) of S_1 to T_n (n = 4, 5 and 6) and T_1 to S_0 (Figure 2D). On the other hand, it should be noted that the RTP population of RTP-D3 (10.6%) is much lower than that of RTP-D2 (70.6%). This is understandable when considering the smaller ISC rate (0.13×10^7 s^{-1} Vs 4.34×10^7 s^{-1}) and phosphorescent radiative decay rate (0.50×10^5 s^{-1} Vs 8.53×10^5 s^{-1}) of RTP-D3 relative to RTP-D2 (Table S2). Accordingly, RTP-D3 is a much weaker emitter (Φ_{PL} = 12.8%) compared with RTP-D2 (Φ_{PL} = 77.5%).

AIEL featured a RTP nature

To evaluate the AIEL featured a RTP nature, namely aggregation-induced electrophosphorescence, RTP-D3 was doped into 1,3-bis(carbazol-9-

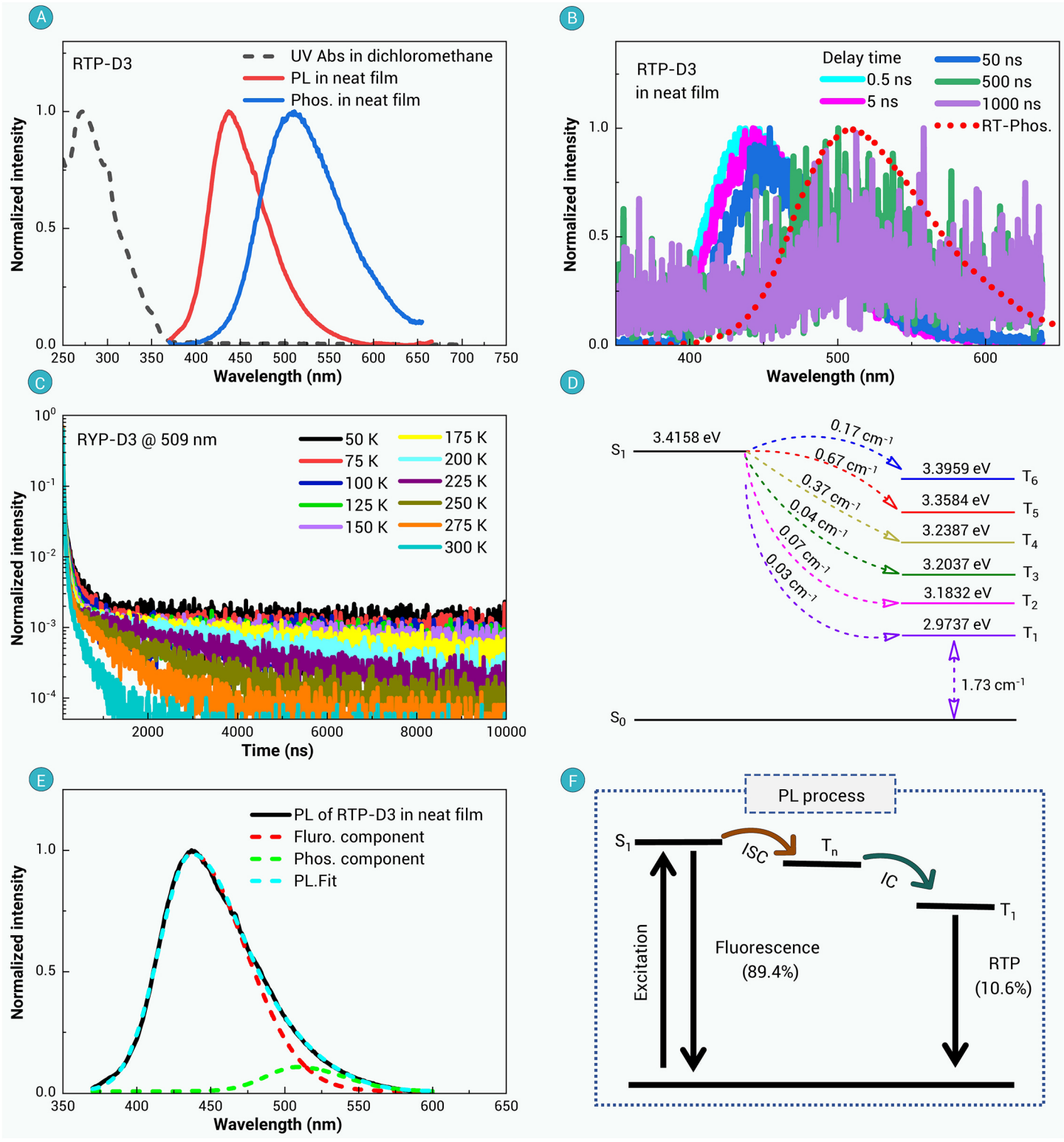

Figure 2. RTP nature of RTP-D3 (A) UV-Vis absorption in dichloromethane, PL (excited at 350 nm) and RTP spectra (excited at 350 nm with a 0.1 ms delay) in neat film; (B) TRES compared with the corresponding RTP; (C) Temperature-dependent transient PL spectra detected at 509 nm; (D) Excited state energies and spin–orbit coupling matrix elements from theoretical calculation; (E) Bigaussian fitting of the PL spectrum in neat film; (F) Proposed PL process.

yl)benzene (mCP) to constitute the emitting layer (EML). And the device structure is ITO/HAT-CN (3 nm)/NPB (40 nm)/TCTA (10 nm)/EML (15 nm)/TmPyPB (50 nm)/Liq (1 nm)/Al (Structure A, Figure S12), where 1,4,5,8,9,11-hexaazatriphenylene hexacarbonitrile (HAT-CN), *N,N'*-Di(1-naphthyl)-*N,N'*-diphenyl-(1,1'-biphenyl)-4,4'-diamine (NPB), tris(4-carbazoyl-9-ylphenyl)amine (TCTA), 1,3,5-tri(m-pyrid-3ylphenyl) benzene (TmPyPB) and 8-Hydroxyquinolinolato-lithium (Liq) serve as the hole injection layer, hole transporting layer, electron blocking layer, electron transporting layer and electron injection layer, respectively.

Different from the PL counterpart (Figure S13), a distinct dual emission appears in the EL (Figure 3A). When the doping concentration is up from 10 to 100 wt.%, the short-wavelength emission at about 419 nm is gradually decreased, accompanied by an enhancement of the long-wavelength emission at about 501 nm. Correspondingly, the CIE coordinates are red-shifted from (0.17, 0.14) to (0.22, 0.38) (Figure 3B). And the EQE and brightness are increased from 1.5% (1.5 cd/A, 1.2 lm/W) and 265 cd/m^2 to 2.4% (5.5 cd/A,

Table 1. Summary of photophysical, electrochemical and thermal properties for RTP-D2 and RTP-D3.

	λ_{abs}[a] [nm]	λ_{PL}[b] [nm]	λ_P[c] [nm]	Φ_{PL}[d] [%]	τ_F/τ_P[e] [ns]	HOMO/LUMO[f] [eV]	S_1/T_1[g] [eV]	ΔE_{ST}[h] [eV]	T_d[i] [°C]	T_g[j] [°C]
RTP-D2	280	497 (91)	505	77.5	12.6/642.7	-5.26/-2.76	2.94/2.73	0.21	351	97
RTP-D3	273	437 (82)	509	12.8	10.5/278.5	-5.42/-2.69	3.19/2.74	0.45	382	91

[a]Absorption measured in 10^{-5} mol L^{-1} dichloromethane solution. [b]PL measured in neat film and the related FWHM values are listed in the parentheses. [c]RTP measured in neat film under a 0.1 ms delay between the pulsed excitation and the emission collection. [d]Film absolute PLQYs measured under N_2 using an integrating sphere. [e]Fluorescence and RTP lifetimes estimated from the transient PL spectra in neat film. [f]HOMO and LUMO levels determined by CV. [g]Energies of S_1 and T_1 are estimated from the onset of PL and RTP spectra, respectively. [h]$\Delta E_{ST} = S_1 - T_1$. [i]Decomposition temperature corresponding to a 5% weight loss. [j]Glass transition temperature taken from the middle value between break points.

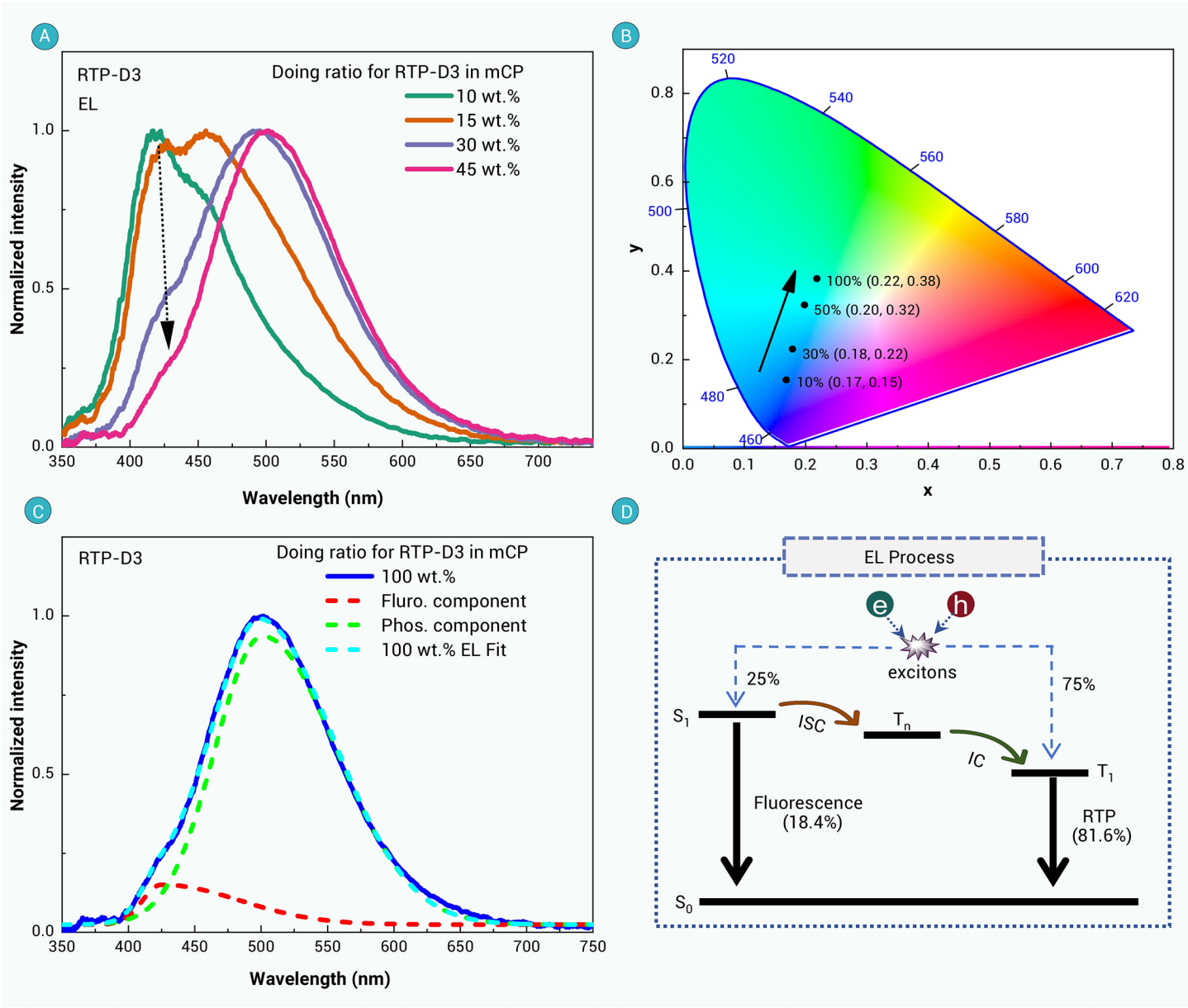

Figure 3. Aggregation-induced electrophosphorescence of RTP-D3 (A) EL spectra with different doping concentration; (B) Related CIE chromaticity diagram; (C) Bigaussian fitting of EL spectrum based on a non-doped device; (D) Proposed EL process.

5.6 lm/W) and 1013 cd/m^2 (Figure S12 & Table S3). According to the literature,[33] the reduced T_1 non-radiative decay, caused by the prevention of the rotation around the C–O single bond under the non-doped condition, is responsible for the obtained aggregation-induced electrophosphorescence. Compared with RTP-D2 (EQE = 15.8%), noticeably, RTP-D3 shows a worse AIEL with a lower EQE of 2.4%, in well agreement with their Φ_{PL}s (12.8% for RTP-D3, and 77.5% for RTP-D2).

As discussed above, the short-wavelength and long-wavelength EL originate from fluorescence and RTP, respectively. Since they can be decoupled from each other, the corresponding populations are able to be estimated easily by comparing their individual integral area (Figure S14 & Table S4). Due to the aggregation-induced electrophosphorescence, the RTP population is significantly enhanced from 17.4 % to 81.6% with the increasing doping concentration in the range of 10-100 wt.%. Taking the non-doped device as

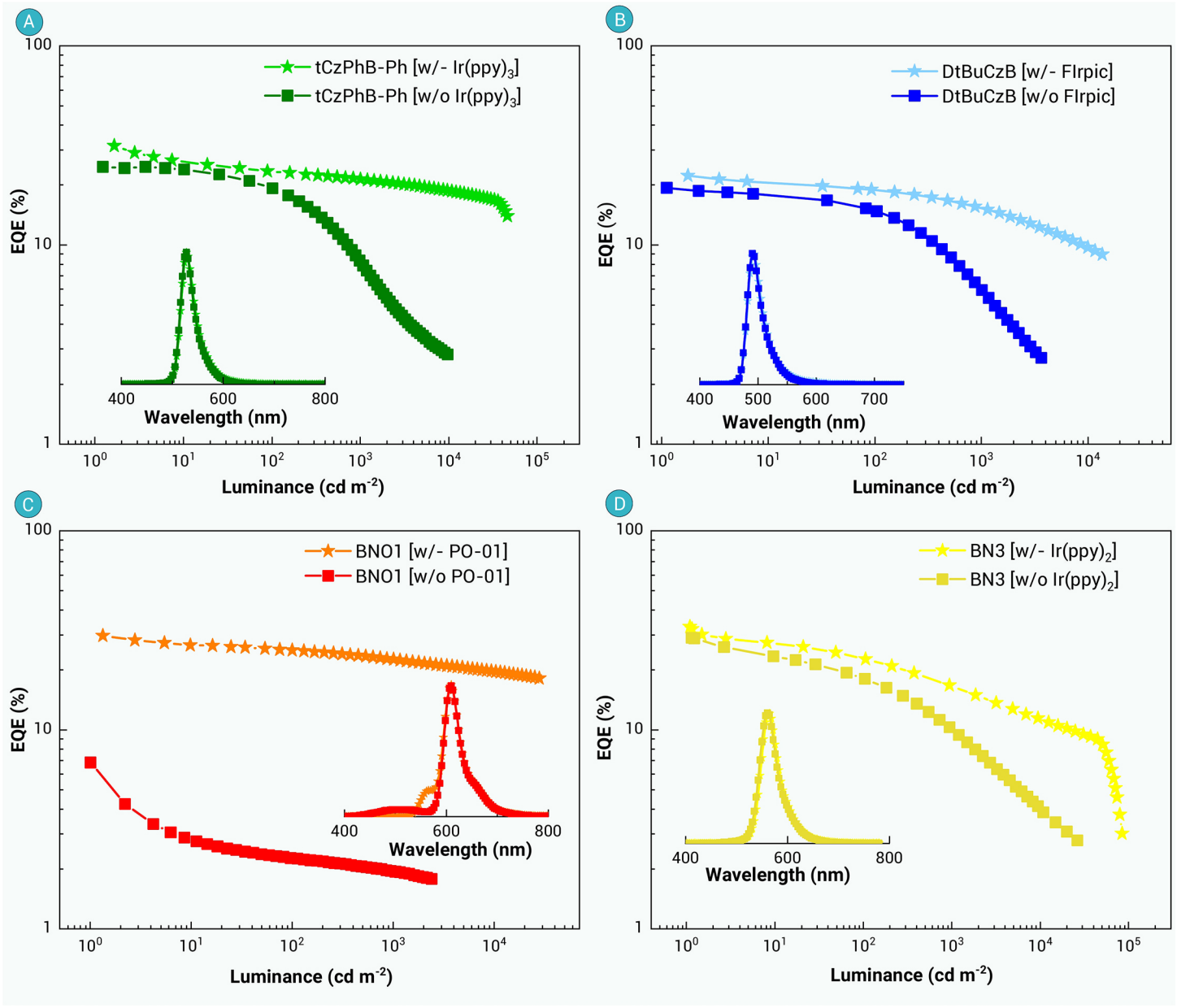

Figure 4. Device performance of matrix-free MR-TADF OLEDs using RTP-D3 as the sensitizer EQE versus luminance characteristics for devices based on four different emitters (A) green emissive tCzPhB-Ph; (B) sky-blue emissive DtBuCzB; (C) red emissive BNO1 and (D) yellow emissive BN3. Inset: EL at 1000 cd/m^2.

an example (Figure 3C), noticeably, the RTP population in the EL (81.6%) turns out to be much higher than that in the PL (10.6%). Under the photo excitation, triplet excitons are formed only through the ISC. Given the relatively small S_1-to-T_n SOCME (0.17-0.67 cm^{-1}), the ISC seems to be inefficient, leading to a weak RTP contribution in the PL process. Nevertheless, under the electrical excitation, most of triplet excitons are generated directly via charge recombination besides ISC (Figure 3D).[37] Because of the relatively large T_1-to-S_0 SOCME (1.73 cm^{-1}), these triplet excitons can be effectively radiative-decayed to produce phosphorescence. Therefore, RTP becomes dominant in the EL process, which is beneficial for the triplet exciton harvesting.

Matrix-free sensitization for MR-TADF emitters

In view of the aggregation-induced electrophosphorescence and high triplet energy of 2.74 eV (Figure S16), RTP-D3 has a great potential in matrix-free sensitization for different color MR-TADF emitters. Aiming at this object, firstly, MR-TADF OLEDs are fabricated based on Structure A, where a BT.2020 green emitter tCzPhB-Ph is dispersed into RTP-D3 at a 2 wt.% content to form the EML in the absence of any additional matrix.[38] Although a narrowband EL is obtained (Figure S17), the device performance (17.3%, 69.8 cd/A and 78.4 lm/W) looks like unsatisfied. So a preferable structure of ITO/HAT-CN (3 nm)/TAPC (35 nm)/TCTA (5 nm)/mCBP (5 nm)/EML (15 nm)/POT2T (10 nm)/ANT-BIZ (40 nm)/Liq (1 nm)/Al (Structure B, Figure S18) is then adopted to optimize the performance of RTP-D3 + tCzPhB-Ph (2 wt.%).[39] Here 4,4′-cyclohexylidenebis[*N*,*N*-bis(4-methylphenyl)aniline] (TAPC) is used as the hole transporting layer instead of NPB, 3,3′-bis(*N*-carbazolyl)-1,1′-biphenyl (mCBP) is inserted between TCTA and EML to realize an efficient hole transporting and an efficient electron blocking, (1,3,5-triazine-2,4,6-triyl)tris(benzene-3,1-diyl))tris(diphenylphosphine oxide) (POT2T) acts as the hole blocking layer, and 1-(4-(10-([1,1′-biphenyl]-4-yl)anthracen-9-yl)phenyl)-2-ethyl-1H-benzo[d]imidazole (ANT-BIZ) is used as the electron transporting layer instead of TmPyPB.

After the device engineering, the maximum current efficiency, power efficiency and EQE have been successfully enhanced to 24.6%, 106.5 cd/A and 119.5 lm/W (Figure 4A & S19), respectively, which are more than doubled those of RTP-D2 (10.8%, 41.5 cd/A and 42.3 lm/W in Figure S20). Such an exceptional result breaks a conventional blind spot, that is, the best sensitizer must be the best emitter. The exciton dynamic analysis (Figure S21) reveals that an efficient FRET can happen from RTP-D3 to tCzPhB-Ph, because the distance between them (2.07 nm) locates below the critical FRET radius of 3.48 nm (Table S5). Although the T_1-to-S_0 non-radiative decay rate is increased for RTP-D3 (k_{nr} = 3.54 × 10^6 s^{-1}) relative to RTP-D2 (k_{nr} = 0.71 × 10^6 s^{-1}), it is still one order magnitude lower than that of the FRET rate (k_{FRET} =

Table 2. Summary of device performance for RTP-D3 sensitized multichromic MR-TADF emitters.

Device		V_{on}[a] [V]	CE[b] [cd/A]	PE[b] [lm/W]	EQE[b] [%]	CIE[c] (x, y)	FWHM [nm]
DtBuCzB	FIrpic (w/o)	2.7	43.3/12.7	50.4/5.1	19.4/6.0	(0.11, 0.47)	29
	FIrpic (w/-)	2.8	49.2/33.7	55.2/16.1	22.2/14.3	(0.12, 0.48)	30
tCzPhB-Ph	$Ir(ppy)_3$ (w/o)	2.8	106.5/33.9	119.5/16.2	24.6/8.2	(0.25, 0.70)	32
	$Ir(ppy)_3$ (w/-)	2.9	105.1/88.1	113.9/51.1	31.5/21.4	(0.26, 0.70)	31
BN3	$Ir(ppy)_2(acac)$ (w/o)	3.1	103.9/39.2	106/32.8	28.9/10.1	(0.43, 0.56)	40
	$Ir(ppy)_2(acac)$ (w/-)	2.7	112.4/63.7	133.3/106.1	32.9/16.3	(0.45, 0.54)	40
BNO1	PO-01 (w/o)	3.4	10.4/3.5	9.7/1.1	6.8/1.9	(0.58, 0.35)	36
	PO-01 (w/-)	2.6	55.4/45.1	66.9/22.9	29.7/22.7	(0.61, 0.39)	38

[a]Turn-on voltage at 1 cd/m^2. [b]Data at maximum and 1000 cd/m^2. [c]At a driving voltage of 6 V. CE: Current Efficiency; PE: Power Efficiency; EQE: External Quantum Efficiency. The doping concentrations are optimized to be 20 wt.% for FIrpic, 3 wt.% for DtBuCzB, 5 wt.% for $Ir(ppy)_3$ and 2 wt.% for tCzPhB-Ph, 4 wt.% for $Ir(ppy)_2(acac)$ and 6 wt.% for BN3, 20 wt.% for PO-01 and 1 wt.% for BNO1.

8.16×10^7 s^{-1}). In this case, triplet excitons tend to transfer their energy to the S_1 of tCzPhB-Ph via a FRET rather than a non-radiative decay (Figure S22). Consequently, RTP-D3 is able to act as a promising sensitizer despite its weak RTP.

According to previously-reported matrix-free sensitization based on TADF, the incorporation of Ir cosensitizer can further improve device performance due to the multiple channels of exciton harvesting.[38,39] Therefore, here *fac*-tris[2-phenylpyridinato-C^2,N]iridium(III) ($Ir(ppy)_3$ is further selected as the cosensitizer because there is a good overlap between the PL of $Ir(ppy)_3$ and the absorption of tCzPhB-Ph to ensure the cascade energy transfer from RTP-D3 to tCzPhB-Ph through $Ir(ppy)_3$ (Figure S23). On the basis of the insensitive current density-voltage behaviors with the varied doping concentration of tCzPhB-Ph (Figure S24), meanwhile, the direct exciton recombination on tCzPhB-Ph is excluded reasonably, thus avoiding the unwanted exciton loss. That is, major singlet and triplet excitons generated on RTP-D3 are able to be transferred first to $Ir(ppy)_3$ and then to the S_1 of tCzPhB-Ph via a FRET and Dexter energy transfer (FRET/DET) route, followed by a fast radiative decay (Figure S25). As a result, the accumulation of triplet excitons and subsequent triplet-triplet annihilation (TTA) could be suppressed, resulting in highly efficient green narrowband EL with a promising EQE as high as 31.5% (105.1 cd/A, 113.9 lm/W), a FWHM of 31 nm and CIE coordinates of (0.26, 0.70). Especially at a high luminance of 1000 cd/m^2, the EQE is greatly increased from 8.2% to 21.4% after the adoption of $Ir(ppy)_3$ as the cosensitizer (Figure 4A & S26).

To evaluate the role of $Ir(ppy)_3$, it is dispersed into a wide-energy gap matrix 4,4′-bis(*N*-carbazolyl)-1,1′-biphenyl (CBP) instead of RTP-D3 to sensitize tCzPhB-Ph by itself. The corresponding device gives a peak EQE of 25.4%, which decays to 17.0% at 1000 cd/m^2 (Figures S27-S28 & Table S6). Noticeably, the obtained performance of CBP: 5 wt.% $Ir(ppy)_3$: 2 wt.% tCzPhB-Ph is worse than that of RTP-D3: 5 wt.% $Ir(ppy)_3$: 2 wt.% tCzPhB-Ph (31.5%@max and 21.4%@1000 cd/m^2), which could be ascribed to the two sensitization processes from $Ir(ppy)_3$ and RTP-D3 simultaneously. This is confirmed by the PL decay curves for CBP: 5 wt.% $Ir(ppy)_3$: 2 wt.% tCzPhB-Ph and RTP-D3: 2 wt.% tCzPhB-Ph (Figure S21). They exhibit shortened exciton lifetimes of sensitizers ($Ir(ppy)_3$ and RTP-D3), indicative of the energy transfer—sensitization—from sensitizer to dopant.[39] Compared with the FRET from $Ir(ppy)_3$ to tCzPhB-Ph ($k_{FRET} = 0.52 \times 10^7$ s^{-1}, $\eta_{FRET} = 77.9\%$), the related rate and efficiency from RTP-D3 to tCzPhB-Ph grow up to be 8.16×10^7 s^{-1} and 95.8%, respectively (Figure S29). As a consequence, both $Ir(ppy)_3$ and RTP-D3 do contribute to the sensitization for the dopant in the case of RTP-D3: 5 wt.% $Ir(ppy)_3$: 2 wt.% tCzPhB-Ph, leading to improved device performance.

Moreover, RTP-D3 is used as the matrix-free sensitizer for other MR-TADF emitters, such as DtBuCzB and BNO1.[40,41] Similar to the green one, high efficiency and small roll-off can be achieved simultaneously in the presence of iridium(III)bis(4,6-di-fluorophenyl)-pyridinato-N,$C^{2'}$)picolinate (FIrpic) and iridium(III) bis(4-phenylthieno[3,2-c]pyridinato-N,$C^{2'}$)acetylacetonate (PO-01). As one can see (Figures 4B-C), DtBuCzB and BNO1 give a bright sky-blue and red narrowband EL, revealing a maximum EQE of 22.2% (49.2 cd/A, 55.2 lm/W) and 29.7% (55.4 cd/A, 66.9 lm/W), a FWHM of 30 nm and 38 nm, as well as CIE coordinates of (0.12, 0.48) and (0.61, 0.39), respectively. And the EQE still remains at 14.3% for DtBuCzB and 22.7% for BNO1 at 1000 cd/m^2, indicative of a gentle efficiency roll-off (Table 2 & Figures S30-S3). The same trend is also observed for the yellow MR-TADF emitter BN3,[42] which shows a promising EQE as high as 32.9% (112.4 cd/A, 133.3 lm/W) accompanied by a FWHM of 40 nm and CIE coordinates of (0.45, 0.54) (Figure 4D & Figures S34-S5). The results clearly illustrate the great potential of RTP-D3 as a universal sensitizer in matrix-free MR-TADF OLEDs.

Although RTP-D3 is weak emissive, it is worth noting that the obtained device performance including efficiency and stability is much better than that of RTP-D2 (Figures S36-S41 & Table S7). Ongoing from RTP-D2 to RTP-D3, the maximum EQE grows up significantly from 12.0%, 20.4%, 21.4% and 24.5% to 22.2%, 31.5%, 32.9% and 29.7% for sky-blue, green, yellow and red devices, respectively (Figure 5A). Except for the unstable blue one, moreover, the green device shows an increased lifetime LT50@1000 cd/m^2 from 77.9 h to 317.8 h, the yellow device shows an increased lifetime LT50@1000 cd/m^2 from 49.4 h to 206.7 h, and the red device shows an increased lifetime LT50@1000 cd/m^2 from 254.6 h to 2431.8 h (Figure 5B). To explain the reason behind, single hole-only and electron-only devices are recorded, and the current density-voltage characteristics are depicted in Figures 5C-D. Compared with RTP-D2, a close hole current and a larger electron current are observed for RTP-D3 at the same voltage. According to a Mott–Gurney law,[43,44] RTP-D2 and RTP-D3 have a comparable hole mobility, while the electron mobility of RTP-D3 is one order magnitude higher than that of RTP-D2 (Figure S42 & Table S8). Such a difference between RTP-D2 and RTP-D3 is consistent with the topology analysis, where RTP-D3 display a much larger electron transfer integral relative to RTP-D2 (Figure S43).

Considering the similar D-O-A geometry, the replacement of acridine by carbazole is believed to contribute to the difference between RTP-D2 and RTP-D3. First, carbazole has a more planar configuration with regard to acridine. Second, benefitting from the weaker donor ability, the electron cloud density located on triazine may be reduced to some degree, thus avoiding the unwanted electrostatic repulsion. Accordingly, a tighter molecular arrangement, especially the triazine fragments, is within our expectation for RTP-D3. In fact, unlike RTP-D2, RTP-D3 displays not only an obvious π-π stacking with a distance of 3.504 Å, but also a strong C-H···π interaction with a distance of 2.770 Å among the triazine units (Figures 5E-F). The closed triazine packing in RTP-D3 is favorable for the electron migration, so that RTP-D3 achieves a more balanced charge transport and thus an improved device efficiency and stability relative to RTP-D2.

CONCLUSION

In summary, a weak emissive organic phosphor named RTP-D3 has been newly designed by selecting carbazole as the D, triazine as the A and oxygen as the bridge between them. Compared with the strong emissive RTP-D2, the replacement of acridine with carbazole is found to enable an extremely poorer AIEL but a more balanced charge transport in RTP-D3. Albeit this, it can be successfully utilized as a universal RTP sensitizer for different color narrowband emitters, achieving an exceptional improved device efficiency and stability. We believe that the present work not only breaks a conventional blind spot about the best sensitizer should be the best emitter, but also provides a guidance for the development of D-O-A organic phosphors capable of matrix-free sensitization in MR-TADF OLEDs.

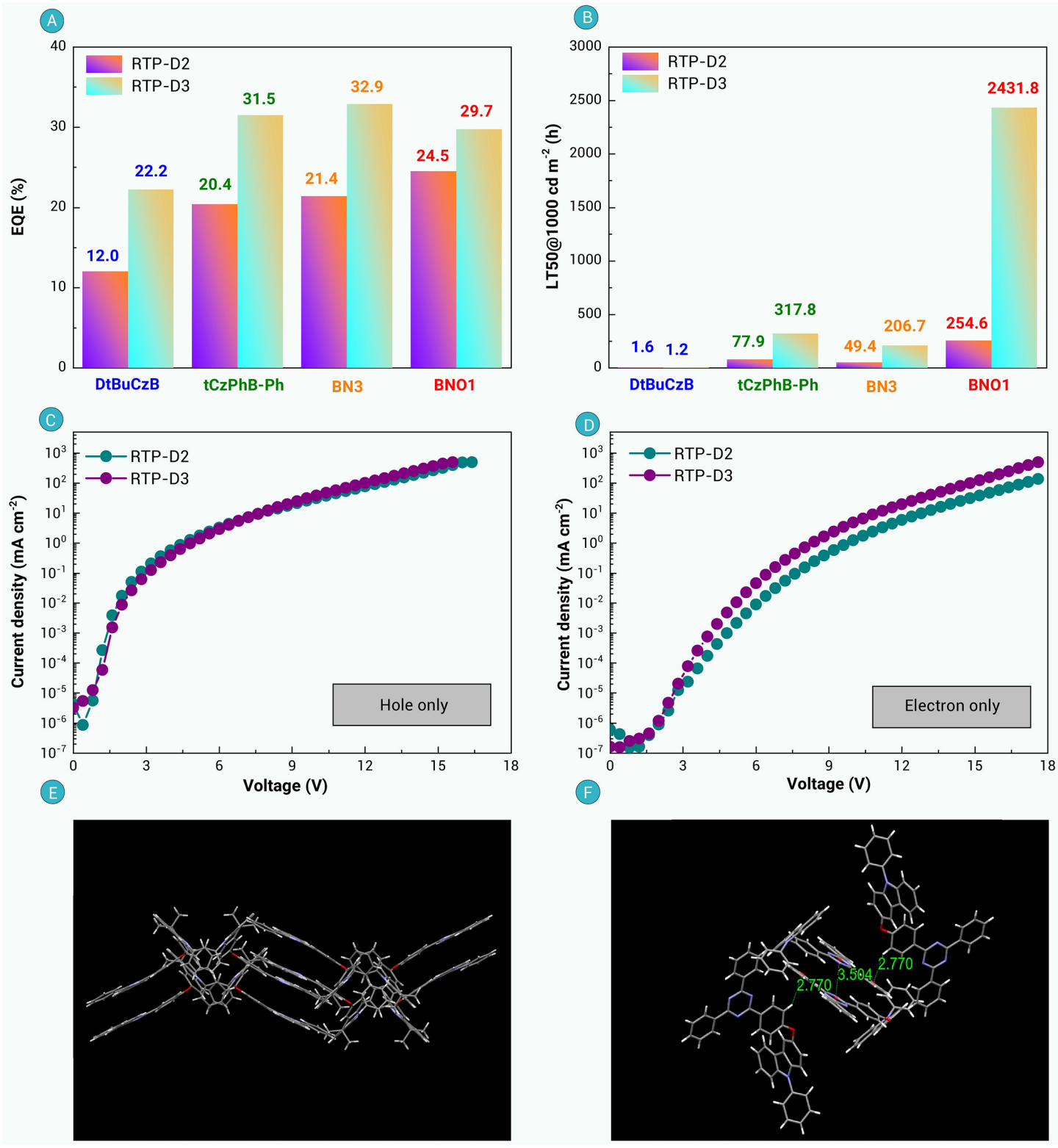

Figure 5. Comparison between RTP-D3 and RTP-D2 (A) Maximum EQE for multichromic MR-TADF emitters; (B) Device lifetime LT50@1000 cd/m^2 for multichromic MR-TADF emitters; (C) Current density–voltage curves for hole-only devices; (D) Current density–voltage curves for electron-only devices; (E) Crystal packing of RTP-D2 with no intermolecular interactions; (F) Crystal packing of RTP-D3, displaying not only an obvious π-π stacking with a distance of 3.504 Å, but also a strong C-H···π interaction with a distance of 2.770 Å among the triazine units.

REFERENCES

1. Hatakeyama T., Shiren K., Nakajima K., et al. (2016). Ultrapure blue thermally activated delayed fluorescence molecules: Efficient HOMO-LUMO separation by the multiple resonance effect. *Adv. Mater.* **28**:2777–2781. DOI:10.1002/adma.201505491
2. Fan X., Hao X., Huang F., et al. (2023). RGB thermally activated delayed fluorescence emitters for organic light-emitting diodes toward realizing the BT.2020 standard. *Adv. Sci.* **10**:2303504. DOI:10.1002/advs.202303504
3. Suresh S. M., Hall D., Beljonne D., et al. (2020). Multiresonant thermally activated delayed fluorescence emitters based on heteroatom-doped nanographenes: Recent advances and prospects for organic light-emitting diodes. *Adv. Funct. Mater.* **30**:1908677. DOI:10.1002/adfm.201908677
4. Kothavale S. S. and Lee J. Y. (2020). Three- and four-coordinate, boron-based, thermally activated delayed fluorescent emitters. *Adv. Opt. Mater.* **8**:2000922. DOI:10.

1002/adom.202000922
5. Kim H. J. and Yasuda T. (2022). Narrowband emissive thermally activated delayed fluorescence materials. *Adv. Opt. Mater.* **10**:2201714. DOI:10.1002/adom.202201714
6. Jiang H., Jin J. and Wong W.-Y. (2023). High-performance multi-resonance thermally activated delayed fluorescence emitters for narrowband organic light-emitting diodes. *Adv. Funct. Mater.* **33**:2306880. DOI:10.1002/adfm.202306880
7. Xu Y., Wang Q., Cai X., et al. (2023). Frontier molecular orbital engineering: Constructing highly efficient narrowband organic electroluminescent materials. *Angew. Chem. Int. Ed.* **62**:e202312451. DOI:10.1002/anie.202312451
8. Kondo Y., Yoshiura K., Kitera S., et al. (2019). Narrowband deep-blue organic light-emitting diode featuring an organoboron-based emitter. *Nat. Photon.* **13**:678–682. DOI:10.1038/s41566-019-0476-5
9. Suresh S. M., Duda E., Hall D., et al. (2020). A deep blue B,N-doped heptacene emitter that shows both thermally activated delayed fluorescence and delayed fluorescence by triplet-triplet annihilation. *J. Am. Chem. Soc.* **142**:6588–6599. DOI:10.1021/jacs.9b13704
10. Xu Y., Li C., Li Z., et al. (2020). Constructing charge-transfer excited states based on frontier molecular orbital engineering: Narrowband green electroluminescence with high color purity and efficiency. *Angew. Chem. Int. Ed.* **59**:17442–17446. DOI:10.1002/anie.202007210
11. Zhang Y., Zhang D., Huang T., et al. (2021). Multi-resonance deep-red emitters with shallow potential-energy surfaces to surpass energy-gap law. *Angew. Chem. Int. Ed.* **60**:20498–20503. DOI:10.1002/anie.202107848
12. Park I. S., Min H. and Yasuda T. (2022). Ultrafast triplet-singlet exciton interconversion in narrowband blue organoboron emitters doped with heavy chalcogens. *Angew. Chem. Int. Ed.* **61**:e202205684. DOI:10.1002/anie.202205684
13. Hu Y. X., Miao J., Hua T., et al. (2022). Efficient selenium-integrated TADF OLEDs with reduced roll-off. *Nat. Photon.* **16**:803–810. DOI:10.1038/s41566-022-01083-y
14. Fan X.-C., Wang K., Shi Y.-Z., et al. (2023). Ultrapure green organic light-emitting diodes based on highly distorted fused π-conjugated molecular design. *Nat. Photon.* **17**:280–285. DOI:10.1038/s41566-022-01106-8
15. Wan D., Zhou J., Meng G., et al. (2024). Peripheral carbazole units-decorated MR emitter containing B–N covalent bond for highly efficient green OLEDs with low roll-off. *J. Semicond.* **45**:082402. DOI:10.1088/1674-4926/24040008
16. Wan D., Zhou J., Yang Y., et al. (2024). Peripheral substitution engineering of MR-TADF emitters embedded with B-N covalent bond towards efficient BT.2020 blue electroluminescence. *Adv. Mater.* **36**:2409706. DOI:10.1002/adma.202409706
17. Zhang Y., Wei J., Zhang D., et al. (2022). Sterically wrapped multiple resonance fluorophors for suppression of concentration quenching and spectrum broadening. *Angew. Chem. Int. Ed.* **61**:e202113206. DOI:10.1002/anie.202113206
18. Zhang D., Song X., Gillett A. J., et al. (2020). Efficient and stable deep-blue fluorescent organic light-emitting diodes employing a sensitizer with fast triplet upconversion. *Adv. Mater.* **32**:1908355. DOI:10.1002/adma.201908355
19. Jeon S. O., Lee K. H., Kim J. S., et al. (2021). High-efficiency, long-lifetime deep-blue organic light-emitting diodes. *Nat. Photon.* **15**:208–215. DOI:10.1038/s41566-021-00763-5
20. Chan C.-Y., Tanaka M., Lee Y.-T., et al. (2021). Stable pure-blue hyperfluorescence organic light-emitting diodes with high-efficiency and narrow emission. *Nat. Photon.* **15**:203–207. DOI:10.1038/s41566-020-00745-z
21. Adachi C. (2014). Third-generation organic electroluminescence materials. *Jpn. J. Appl. Phys.* **53**:060101. DOI:10.7567/JJAP.53.060101
22. Liu Y., Li C., Ren Z., et al. (2018). All-organic thermally activated delayed fluorescence materials for organic light-emitting diodes. *Nat. Rev. Mater.* **3**:18020. DOI:10.1038/natrevmats.2018.20
23. Cai M., Zhang D. and Duan L. (2019). High performance thermally activated delayed fluorescence sensitized organic light-emitting diodes. *Chem. Rec.* **19**:1611–1623. DOI:10.1002/tcr.201800148
24. Chen J., Liu H., Guo J., et al. (2022). Robust luminescent molecules with high-level reverse intersystem crossing for efficient near ultraviolet organic light-emitting diodes. *Angew. Chem. Int. Ed.* **61**:e202116810. DOI:10.1002/anie.202116810
25. Cho H.-H., Congrave D. G., Gillett A. J., et al. (2024). Suppression of Dexter transfer by covalent encapsulation for efficient matrix-free narrowband deep blue hyperfluorescent OLEDs. *Nat. Mater.* **23**:519–526. DOI:10.1038/s41563-024-01812-4
26. Zhang D., Duan L., Li C., et al. (2014). High-efficiency fluorescent organic light-emitting devices using sensitizing hosts with a small singlet-triplet exchange energy. *Adv. Mater.* **26**:5050–5055. DOI:10.1002/adma.201401476
27. Cho H.-H., Romanov A. S., Bochmann M., et al. (2021). Matrix-free hyperfluorescent organic light-emitting diodes based on carbene-metal-amides. *Adv. Opt. Mater.* **9**:2001965. DOI:10.1002/adom.202001965
28. Zhang Q., Tsang D., Kuwabara H., et al. (2015). Nearly 100% internal quantum efficiency in undoped electroluminescent devices employing pure organic emitters. *Adv. Mater.* **27**:2096–2100. DOI:10.1002/adma.201405474
29. Li X., Yan L., Liu S., et al. (2023). Polymerized thermally activated delayed-fluorescence small molecules: Long-axis polymerization leads to a nearly concentration-independent luminescence. *Angew. Chem. Int. Ed.* **62**:e202300529. DOI:10.1002/anie.202300529
30. Su N., Chen B. and Ding J. (2024). Two birds with one stone: polymerized thermally activated delayed fluorescence small molecules. *Chem. Eur. J.* **30**:e202304095. DOI:10.1002/chem.202304095
31. Zhao W., He Z. and Tang B. Z. (2020). Room-temperature phosphorescence from organic aggregates. *Nat. Rev. Mater.* **5**:869–885. DOI:10.1038/s41578-020-0223-z
32. Liu X., Yang L., Li X., et al. (2021). An electroactive pure organic room-temperature phosphorescence polymer based on a donor-oxygen-acceptor geometry. *Angew. Chem. Int. Ed.* **60**:2455–2463. DOI:10.1002/anie.202011957
33. Xu L., Mo Y., Su N., et al. (2023). D-O-A based organic phosphors for both aggregation-induced electrophosphorescence and host-free sensitization. *Nat. Commun.* **14**:1678. DOI:10.1038/s41467-023-37414-y
34. Stavrou K., Franca L. G., Danos A., et al. (2024). Key requirements for ultraefficient sensitization in hyperfluorescence organic light-emitting diodes. *Nat. Photon.* **18**:554–561. DOI:10.1038/s41566-024-01395-1
35. El-Sayed M. A. (1963). Spin-orbit coupling and the radiationless processes in nitrogen heterocyclics. *J. Chem. Phys.* **38**:2834–2838. DOI:10.1063/1.1733610
36. Lee D. R., Lee K. H., Shao W., et al. (2020). Heavy atom effect of selenium for metal-free phosphorescent light-emitting diodes. *Chem. Mater.* **32**:2583–2592. DOI:10.1021/acs.chemmater.0c00078
37. Baldo M. A., O'Brien D. F., Thompson M. E., et al. (1999). Excitonic singlet-triplet ratio in a semiconducting organic thin film. *Phys. Rev. B.* **60**:14422. DOI:10.1103/PhysRevB.60.14422
38. Liu J., Zhu Y., Tsuboi T., et al. (2022). Toward a BT.2020 green emitter through a combined multiple resonance effect and multi-lock strategy. *Nat. Commun.* **13**:4876. DOI:10.1038/s41467-022-32607-3
39. Chen Y., Zhang Y., Huang T., et al. (2022). Highly efficient and nearly roll-off–free electrofluorescent devices via multiple sensitizations. *Sci. Adv.* **8**:eabp9203. DOI:10.1126/sciadv.abp9203
40. Zou Y., Hu J., Yu M., et al. (2022). High-performance narrowband pure-red OLEDs with external quantum efficiencies up to 36.1% and ultralow efficiency roll-off. *Adv. Mater.* **34**:2201442. DOI:10.1002/adma.202201442
41. Xu Y., Cheng Z., Li Z., et al. (2020). Molecular-structure and device-configuration optimizations toward highly efficient green electroluminescence with narrowband emission and high color purity. *Adv. Opt. Mater.* **8**:1902142. DOI:10.1002/adom.201902142
42. Qi Y., Ning W., Zou Y., et al. (2021). Peripheral decoration of multi-resonance molecules as a versatile approach for simultaneous long-wavelength and narrowband emission. *Adv. Funct. Mater.* **31**:2102017. DOI:10.1002/adfm.202102017
43. Blom P. W. M., de Jong M. J. M. and Vleggaar J. J. M. (1996). Electron and hole transport in poly(*p*-phenylene vinylene) devices. *Appl. Phys. Lett.* **68**:3308–3310. DOI:10.1063/1.116583
44. Chen C.-H., Lin S.-C., Lin B.-Y., et al. (2022). New bipolar host materials for high power efficiency green thermally activated delayed fluorescence OLEDs. *Chem. Eng. J.* **442**:136292. DOI:10.1016/j.cej.2022.136292

FUNDING AND ACKNOWLEDGMENTS

The authors acknowledge the financial support from the National Natural Science Foundation of China (No. 52273198), Yunnan Fundamental Research Projects (No. 202301BF070001-008) and the Yunling Scholar Project of "Yunnan Revitalization Talent Support Program". Dr. Ning Sun thanks Yunnan Province Basic Research Project (No. 202301AT070221). We thank Prof. Chuluo Yang (Shenzhen University) and Dr. Qisheng Zhang (Zhejiang Hongwu Technology Co. Ltd.) to provide BNO1 and tCzPhB-Ph at the early stage of matrix-free sensitization based on D-O-A organic phosphors. We also thank Advanced Analysis and Measurement Center of Yunnan University for the assistance with instrumentation. The funders had no role in study design, data collection and analysis, decision to publish, or preparation of the manuscript.

AUTHOR CONTRIBUTIONS

L.X. and S.X. contributed equally to this study. L.D. and J.D. conceived and supervised the project. L.X. and S.X. performed most of the experiments and analyses. Y.Y. assisted with most of the testing work. C.S., H.D. and N.S. performed the device preparation and guided the data analysis. L.X., H.S., L.D. and J.D. wrote and revised the manuscript. All authors contributed to the manuscript and approved the final version.

DECLARATION OF INTERESTS

The authors declare no competing interests.

DATA AND CODE AVAILABILITY

All data supporting the findings of this study are available from the corresponding author upon reasonable request.

SUPPLEMENTAL INFORMATION

It can be found online at 10.59717/j.xinn-mater.2026.100210.